

Influence of excitation and deexcitation processes on the dynamics of laser-excited argon clusters

M. Moll and M. Schlanges

Institut für Physik, Universität Greifswald, D-17487 Greifswald, Germany

Th. Bornath*

Institut für Physik, Universität Rostock, D-18051 Rostock, Germany

V. P. Krainov

Moscow Institute for Physics and Technology, 141700 Dolgoprudny, Moscow Region, Russia

(Received 21 November 2014; published 18 March 2015)

The excitation of atomic clusters by intense infrared laser pulses leads to the creation of highly charged ions and to the emission of energetic photons. These phenomena, which follow from ionization processes occurring in the cluster, depend significantly on the population of ground states and excited states in the laser-produced nanoplasma. This makes it necessary to account for collisional excitation and deexcitation processes. We investigate the interaction of femtosecond laser pulses with argon clusters by means of a nanoplasma model. Considering laser excitation with single and double pulses, we analyze the role of excitation and deexcitation processes in detail and calculate the yield of highly charged ions and of energetic photons in different wavelength regimes.

DOI: [10.1103/PhysRevA.91.033405](https://doi.org/10.1103/PhysRevA.91.033405)

PACS number(s): 36.40.Gk, 31.70.Hq, 52.25.Jm, 52.50.Jm

I. INTRODUCTION

A very prominent method to produce plasmas with a high density and high temperature is the laser excitation of nanometer-sized atomic clusters. Starting with lasers operating in the infrared (IR) regime, characteristic features occurring in the laser-cluster interaction have been observed such as x-ray emission [1,2] and the generation of high-order harmonics [3,4], highly charged ions [5,6], and energetic electrons [7–9]. Resulting from the progress in laser technology, the extensive investigation of the laser-cluster interaction with IR laser fields [10–12] was later extended to laser radiation in the ultraviolet regime [13,14], and it is nowadays possible to perform experiments even with x-ray photons [15,16] due to the advent of free electron lasers. With the high-energetic photons provided by free electron lasers, it is possible to produce ions with very high charge states such as Kr^{21+} [17] and Xe^{36+} [18] from the laser excitation of individual atoms. However, ions with high charge states have also been observed in laser-cluster experiments in the IR regime, where the photon energy is much lower than the binding energy of the cluster atoms. In these experiments, the ionization of the atoms up to high charge states is due to collective effects occurring in the cluster [19]. Of particular importance is the Mie resonance, in which the heating of the nanoplasma via inverse bremsstrahlung [20–22] is increased due to collective excitations of the free electrons inside the cluster [10,11].

There exists a variety of approaches for the theoretical description and simulation of the laser-cluster interaction. In the case of smaller clusters where the particle number is not too large, classical molecular dynamics (MD) simulations [23–27] can be used. A quantum-classical hybrid description combining classical MD with a Monte Carlo scheme to

include quantum ionization rates was used in [28]. For larger clusters, either MD calculations using a hierarchical tree code [19] or particle-in-cell (PIC) simulations [29–31] (including the microscopic PIC method MicPIC [32,33]) are appropriate. Quite another method to theoretically investigate the laser-cluster interaction in the case of larger clusters is hydrodynamic modeling [5,34,35] which is based on the assumption that the laser-excited cluster is transformed into a small, dense plasma. In these nanoplasmas, collective effects become important, which essentially determine the cluster dynamics. Such effects are accounted for, in particular, in the nanoplasma model introduced by Ditmire *et al.* [5] and its modifications [36–39]. Within this model, the clusters are treated as small plasma balls with spherical geometry during all stages of the laser-cluster interaction, which is described by means of a set of coupled hydrodynamic equations and rate equations.

Although the basic physical mechanisms which determine the interaction of atomic clusters with IR laser fields are understood, it is still a demanding task to provide a complete description of all the relevant processes underlying the laser-cluster interaction. It was shown by Micheau *et al.* [38] that the inclusion of excitation processes in a nanoplasma model resulted in an enhanced ionization dynamics and thus in the production of experimentally observed highly charged ions. An augmented collisional ionization from two-step ionization processes leading to increased charge states was also found by Ackad *et al.* [40], who simulated the interaction of small argon clusters with ultraviolet laser pulses with an MD code. In these previous works, collisional excitation processes were included, but the inverse process, collisional deexcitation, was neglected. However, because the rates for collisional excitation and deexcitation are typically of the same order of magnitude [41], collisional deexcitation plays a crucial role for the correct description of the population of ground states and excited states. This is of particular importance in order to investigate the photon emission from laser-excited clusters,

*thomas.bornath@uni-rostock.de

which results from noncollisional transitions between excited states and ground states.

It is the aim of this paper to investigate the interaction of argon clusters with IR laser fields by taking into account collisional excitation and—in addition to the nanoplasma calculations performed in [38]—deexcitation processes and to analyze their influence on the dynamics of the laser-cluster interaction within a nanoplasma model. This model is suitable for clusters with an initial radius $\gtrsim 5$ nm; for smaller clusters, surface effects start to dominate and the hydrodynamic description breaks down. On the other hand, the cluster radius must not be considerably larger than the skin depth. With the nanoplasma model, the temporal evolution of different plasma parameters is analyzed in detail, which includes the population of charge states, the electron temperature and density, and the laser-produced internal field inside the cluster. The physical mechanisms underlying the model and their theoretical description are introduced and results from a ground-state model—in which excited states are neglected—are discussed in Sec. II. By going beyond the ground-state model, both excitation and deexcitation processes are included in our nanoplasma model in Sec. III. Results from this extended model are presented, and the effect of excitation and deexcitation processes on the ionization dynamics and on the different plasma parameters is examined. Moreover, the influence of excited states on the double-pulse excitation of argon clusters is investigated. As the subject of Sec. IV, the emission of radiation is considered and the photon yield is calculated for different interionic transitions and different photon energies. Starting with photon emission stemming from excited electrons on outer ionic shells, we also consider x-ray emission due to inner-shell excitations and compare our results with theoretical results and a measured spectrum from [38]. Finally, in Sec. V, conclusions are drawn.

II. THE GROUND-STATE MODEL

A. Tunnel ionization

In the nanoplasma model, the laser field is described in the dipole approximation, and monochromatic Gaussian laser pulses are considered, with the time-dependent laser intensity $I(t)$ having the form

$$I(t) = I_0 \exp \left\{ -\frac{4 \ln 2}{\tau^2} t^2 \right\}, \quad (1)$$

where I_0 is the peak intensity, and τ is the full width at half-maximum of the pulse. The laser-field amplitude E_0 is given from the intensity and the speed of light in vacuum according to $E_0 = \sqrt{8\pi I/c}$. In the presence of the external laser pulse, the first free electrons are created in the system due to tunnel ionization. As in [5], we use the tunnel ionization rates of Amosov, Delone, and Krainov [42],

$$W_{\text{tunnel}}^{(Z)} = \omega_a C_{n^*l^*}^2 G_{lm} \left(\frac{3E_{\text{int}}}{\pi(2I_Z)^{3/2}} \right)^{1/2} I_Z \times \exp \left\{ -\frac{2(2I_Z)^{3/2}}{3E_{\text{int}}} \right\} \left(\frac{2(2I_Z)^{3/2}}{E_{\text{int}}} \right)^{2n^*-|m|-1}, \quad (2)$$

in which I_Z is the binding energy of the atom or ion before the tunneling in units of 27.2 eV, E_{int} is the electric field inside the cluster (which is in general not identical to E_0 ; see below) in units of 5.14×10^{11} V/m, and $\omega_a = 4.16 \times 10^{16}$ Hz. The coefficients appearing in (2) are

$$G_{lm} = \frac{(2l+1)(l+|m|)!}{2^{|m|}|m|!(l-|m|)!} \quad (3)$$

and

$$C_{n^*l^*}^2 = \frac{2^{2n^*}}{n^* \Gamma(n^* - l^*) \Gamma(n^* + l^* + 1)}, \quad (4)$$

where Γ denotes the gamma function, and l and m are the orbital and magnetic quantum number of the tunneling electron, respectively. Besides, effective quantum numbers are given as $n^* = Z(2I_{Z-1})^{-1/2}$ and $l^* = n_0^* - 1$ if $l \neq 0$ and $l^* = 0$ if $l = 0$, with Z being the charge state of the ion after the tunneling and n_0^* being the effective principal quantum number of the lowest state for a given l [43].

B. Ionization by electron impact

The free electrons in the cluster extract energy from the laser field via inverse bremsstrahlung, which results in persistent heating of the cluster accompanied by further ionization via electron impact. Here we follow [5] and use, for the electron impact ionization, simplified Lotz cross sections [44] of the form

$$\sigma_{\text{ion}}^{(Z)} = a q \frac{\ln(E/I_Z)}{E I_Z} \Theta(E - I_Z), \quad (5)$$

in which I_Z is the ionization energy of an atom or ion with charge state Z , E is the energy of the impinging electron, q is the number of electrons in the outermost shell, and $a = 4.5 \times 10^{-14} \text{ cm}^2 (\text{eV})^2$. Micheau *et al.* [38] introduced a numerical method for the determination of a unique electron-ion collisional ionization rate accounting simultaneously for both the thermal motion of the electrons and their laser-induced motion. To apply a corresponding analytical expression, we consider the decomposition of the electron momentum [38]

$$\mathbf{p}_e = \mathbf{p} + \mathbf{p}_{\text{os}}(t), \quad (6)$$

where $\mathbf{p}_{\text{os}}(t) = e\mathbf{E}_{\text{int}} \cos(\omega t)/\omega$ is the momentum due to the oscillating field with amplitude \mathbf{E}_{int} inside the cluster. Due to the high density of free electrons, the collisionality in the nanoplasma is very high. Thus, it can be assumed that no temperature or density gradients exist and that the “thermal” momentum \mathbf{p} is distributed according to a Maxwell-Boltzmann distribution with electron temperature T_e ,

$$f(\mathbf{p}) = \left(\frac{1}{2\pi m_e k_B T_e} \right)^{3/2} \exp \left\{ -\frac{p^2}{2m_e k_B T_e} \right\}, \quad (7)$$

with $\int d^3p f(\mathbf{p}) = 1$ and k_B being the Boltzmann constant. As usual [45], the rate for impact ionization is obtained by averaging the product of the ionization cross section and the velocity of the impinging electron with respect to the distribution function $f(\mathbf{p})$. In the presence of the laser field, this product is $v_e \sigma_{\text{ion}}^{(Z)}(v_e)$, with the velocity $\mathbf{v}_e = \mathbf{p}_e/m_e$ given by means of (6). By averaging over one oscillation period T ,

the field-dependent ionization rate for electron impact is given as

$$W_{\text{coll}}^{(Z)} = n_e \frac{1}{T} \int_0^T dt \int d^3 p f(\mathbf{p}) \frac{p_e}{m_e} \sigma_{\text{ion}}^{(Z)}(p_e), \quad (8)$$

with n_e being the number density of the free electrons. By substituting the integration variable in (8) with the help of (6), one obtains

$$\begin{aligned} W_{\text{coll}}^{(Z)} &= \frac{n_e}{T} \int_0^T dt \int d^3 p_e f(\mathbf{p}_e - \mathbf{p}_{\text{os}}(t)) \frac{p_e}{m_e} \sigma_{\text{ion}}^{(Z)}(p_e) \\ &= \frac{4n_e k_B T_e}{(2\pi m_e k_B T_e)^{3/2}} \int_0^\pi d\varphi \int_{p_{\text{ion}}}^\infty dp_e p_e^2 \sigma_{\text{ion}}^{(Z)}(p_e) \\ &\quad \times \frac{\sinh\left(\frac{p_e e E_{\text{int}} \cos \varphi}{\omega m_e k_B T_e}\right)}{\frac{e E_{\text{int}}}{\omega} \cos \varphi} \exp\left\{-\frac{p_e^2 + \frac{e^2 E_{\text{int}}^2}{\omega^2} \cos^2 \varphi}{2m_e k_B T_e}\right\}, \quad (9) \end{aligned}$$

in which $p_{\text{ion}} = \sqrt{2m_e I_Z}$, and we substituted $\varphi = \omega t$.

C. Lowering of the ionization energies

An important effect occurring in dense plasmas is the lowering of the ionization energies due to the plasma medium [46]. For bulk plasmas and cross sections of the type of (5), a simple relation between the ionization rate for isolated atoms or ions, W_{ideal} , and the effective ionization rate, W_{eff} , accounting for many-particle effects in the plasma was found to be [47]

$$W_{\text{eff}} = W_{\text{ideal}} \exp\left\{\frac{\Delta E^{(Z)}}{k_B T}\right\}, \quad (10)$$

where the energy shift $\Delta E^{(Z)}$ describes the lowering of the ionization energy I_{Z-1} of an atom or ion with charge $(Z-1)$ according to

$$I_{Z-1}^{\text{eff}} = I_{Z-1} - \Delta E^{(Z)}. \quad (11)$$

Thus, the lowering of the ionization energy leads to an increase in the ionization rate. An expression for the energy shift $\Delta E^{(Z)}$ due to Stewart and Pyatt [48] is

$$\Delta E_{\text{SP}}^{(Z)} = \frac{k_B T_e}{2} \left\{ \left[\left(\frac{a_Z}{r_D} \right)^3 + 1 \right]^{2/3} - 1 \right\}, \quad (12)$$

which was found by interpolating between the Debye screening model, with Debye radius $r_D = [k_B T_e / (4\pi n_e e^2)]^{1/2}$, and the ion sphere model, with $a_Z = [3Z / (4\pi n_e)]^{1/3}$ being the radius of the ion sphere. Similarly to [37] and [39], we use here relation (10) together with the shift, (12), for the lowering of the ionization energies considering tunnel ionization and collisional ionization in the framework of the nanoplasma model.

D. Cluster expansion

The laser-excited nanoplasma expands during and after the laser pulse due to (i) the pressure associated with the hot electrons and (ii) the charge buildup that is created when electrons leave the cluster (outer ionization). As a consequence, the electrons spread and pull the cold, much heavier ions with them, thus causing the whole cluster to

expand, which leads to a cooling of the system. The temporal evolution of the cluster radius R is given as [37,49]

$$\frac{d^2 R}{dt^2} = \frac{5}{R} \frac{P_e + P_{\text{Coul}}}{m_i n_i}, \quad (13)$$

in which m_i is the mass of the plasma ions and n_i the ionic number density. Moreover, P_e is the thermal pressure of the electrons and P_{Coul} denotes the Coulomb pressure due to the outer ionization. The former is given from the chemical potential of the electrons, μ_e —which can be calculated from n_e and T_e with a simple interpolation formula [46]—according to

$$P_e = 2k_B T_e \left(\frac{m_e k_B T_e}{2\pi \hbar^2} \right)^{3/2} I_{3/2} \left(\frac{\mu_e}{k_B T_e} \right) \quad (14)$$

by means of the Fermi integral $I_{3/2}(x)$. In the case of an ideal classical electron gas (for $|x| \rightarrow \infty$), Eq. (14) reduces to

$$P_e = n_e k_B T_e. \quad (15)$$

In order to estimate the Coulomb pressure, Ditmire *et al.* assumed that the associated charge buildup $+Qe$ accumulates on the surface of the spherical cluster, yielding [5]

$$P_{\text{Coul}} = \frac{Q^2 e^2}{8\pi R^4}. \quad (16)$$

E. Cluster heating

The internal energy of the electrons in the laser-excited cluster, U_{int} , changes during the laser-cluster interaction as a result of different physical mechanisms. Its temporal evolution is given as

$$\begin{aligned} \frac{d}{dt} U_{\text{int}} &= \dot{U}_{\text{laser}} - \dot{U}_{\text{exp}} - \dot{U}_{\text{surf}} \\ &\quad - \sum_Z (I_{Z-1} - \Delta E_{\text{SP}}^{(Z)}) \frac{dN_Z}{dt} \Big|_{Z-1 \rightarrow Z}, \quad (17) \end{aligned}$$

where \dot{U}_{laser} is the change of the internal energy due to the laser heating, the term $-\dot{U}_{\text{exp}} = 4\pi R^2 P_e dR/(dt)$ denotes the change due to the cluster expansion [5], and the energy loss by electron flow through the cluster surface is denoted $-\dot{U}_{\text{surf}}$. Moreover, the last term describes the electron energy loss in ionization processes, and we neglected the energy transfer from the electrons to the slow, cold ions, because it is unimportant on the time scale of the plasma heating by the laser pulse [5]. By setting $U_{\text{int}} = \frac{3}{2} N_e k_B T_e$, the left-hand side of (17) becomes

$$\frac{d}{dt} U_{\text{int}} = \frac{3}{2} k_B \left(N_e \frac{\partial T_e}{\partial t} + T_e \frac{\partial N_e}{\partial t} \right). \quad (18)$$

The change in the number of free electrons in the cluster, N_e , is determined (i) by inner ionization of the atoms and ions inside the cluster and (ii) by electrons leaving the cluster as a whole (outer ionization):

$$\begin{aligned} \frac{3}{2} k_B T_e \frac{\partial N_e}{\partial t} &= \frac{3}{2} k_B T_e \sum_Z \frac{\partial N_Z}{\partial t} \Big|_{Z-1 \rightarrow Z} \\ &\quad - \frac{3}{2} k_B T_e \frac{\partial N_e}{\partial t} \Big|_{\text{outer ioniz.}}. \quad (19) \end{aligned}$$

The last term on the right-hand side of (19) can be identified with $-\dot{U}_{\text{surf}}$ in (17), and the two terms cancel each other out. After inserting the electron pressure, (15), the equation for the temperature evolution becomes

$$\frac{\partial T_e}{\partial t} = -\frac{2T_e}{R} \frac{dR}{dt} + \frac{1}{C} \left\{ \dot{U}_{\text{laser}} - \sum_Z \frac{dN_Z}{dt} \Big|_{Z-1 \rightarrow Z} \times \left(\frac{3}{2} k_B T_e + I_{Z-1} - \Delta E_{\text{SP}}^{(Z)} \right) \right\}, \quad (20)$$

with the heat capacity $C = \frac{3}{2} N_e k_B$.

For clusters with a spherical shape and macroscopic dielectric function $\varepsilon(\omega)$, one finds that the external field E_0 is screened, resulting in an internal field [50]

$$E_{\text{int}} = \frac{3}{|\varepsilon(\omega) + 2|} E_0, \quad (21)$$

and within a simple Drude model, one obtains

$$E_{\text{int}} = \left(\frac{\omega^2 + \nu^2}{(\omega - \frac{\omega_p^2}{3\omega})^2 + \nu^2} \right)^{1/2} E_0, \quad (22)$$

with the plasma frequency $\omega_p = [4\pi n_e e^2 / m_e]^{1/2}$. The denominator in (22) is minimized—and therefore, the internal field is resonantly increased compared to the external field—if the condition $\omega = \omega_p / \sqrt{3}$ is fulfilled. This is due to the collective excitation of Mie surface plasmons, which is denoted the Mie resonance. Analogously, the heating term in (20) can be written as [5]

$$\frac{1}{C} \dot{U}_{\text{laser}} = \frac{e^2 E_0^2}{3k_B m_e} \frac{\nu(\omega)}{(\omega - \frac{\omega_p^2}{3\omega})^2 + \nu^2(\omega)}, \quad (23)$$

showing the same resonant behavior. The heating of the electrons by the laser field is mainly due to inverse bremsstrahlung via electron-ion collisions. The inverse bremsstrahlung heating rate can be expressed by means of the electron-ion collision frequency ν_{ei} , for which we use a quantum statistical expression [39,51],

$$\nu_{ei}(\omega) = \frac{4\bar{Z}^2 n_i m_e \omega^3}{n_e e^2 E_{\text{int}}^2} \sum_{n=1}^{\infty} n \int \frac{d^3 q}{(2\pi \hbar)^3} V(q) S_{ii}(q) \times \frac{\text{Im} \varepsilon(q, n\omega)}{|\varepsilon(q, n\omega)|^2} J_n^2 \left(\frac{\mathbf{q} \cdot \mathbf{E}_{\text{int}} e}{m_e \hbar \omega^2} \right). \quad (24)$$

In this expression, $\varepsilon(q, \omega)$ is the dielectric function of the electronic subsystem, J_n are Bessel functions, \bar{Z}^2 is the mean squared ionic charge state in the cluster, and $V(q) = 4\pi \hbar^2 e^2 / q^2$. Moreover, the electric-field amplitude \mathbf{E}_{int} in (24) is the internal field inside the cluster where the electron-ion collisions occur, and S_{ii} is the ion-ion structure factor, which is here set to unity.

The electron-ion collisions are responsible for a damping of the Mie surface plasmons, which are due to dipolar oscillations of the spherical cluster surface [52]. The coherence of the plasmon oscillations can be reduced by random collisions of the cluster electrons with the surface [53], which leads to an additional damping. To account for this effect, we follow [36],

introducing an additional collision frequency of the form

$$\nu_s = \frac{\bar{v}}{R}, \quad (25)$$

where we take the velocity \bar{v} from the mean kinetic energy \bar{E}_{kin} of free electrons in the laser field,

$$\bar{E}_{\text{kin}} = \frac{m_e}{2} \bar{v}^2 = \frac{3}{2} k_B T_e + U_p, \quad (26)$$

with the ponderomotive potential $U_p = e^2 E_{\text{int}}^2 / (4m_e \omega^2)$, which is the energy of a free electron averaged over one laser cycle. The collision frequency ν in (23) is thus determined by electron-ion collisions as well as by collisions with the cluster surface:

$$\nu = \nu_{ei} + \nu_s. \quad (27)$$

Because ν_{ei} and U_p depend on the internal field inside the cluster and the internal field depends on ν_{ei} according to (22), these quantities are calculated self-consistently. If ν is of the order of ω , the Drude model starts to lose its validity. Hence, in the case $\nu \gg \omega$, a different numerical prefactor occurs on the right-hand side of (23) [10]. However, because our numerical calculations show that the cluster evolution is not sensitive to this effect, we always use (23) to describe the cluster heating.

F. Plasma composition

The atoms in the initially neutral cluster are continually ionized to higher ionic charge states under the influence of the laser field either by tunnel ionization or by electron-impact ionization. The system of rate equations describing the temporal evolution of the total numbers N_i of atoms ($i = 0$) and ions ($i \geq 1$) is given as

$$\begin{aligned} \frac{dN_0}{dt} &= -W_0 N_0, \\ \frac{dN_i}{dt} &= W_{i-1} N_{i-1} - W_i N_i, \quad i = 1, \dots, Z_n - 1, \\ \frac{dN_{Z_n}}{dt} &= W_{Z_n-1} N_{Z_n-1}, \end{aligned} \quad (28)$$

where Z_n denotes the nuclear charge, and only atoms or ions in the ground state are considered. The quantity W_i , which is the rate for ionization from charge state i to charge state $(i + 1)$, is given as the sum of the rate for tunnel ionization, (2), and the rate for collisional ionization, (9),

$$W_i = W_{\text{tunnel}}^{(i)} + W_{\text{coll}}^{(i)}. \quad (29)$$

Taking into account the lowering of the ionization energies, these rates are modified with the respective Stewart-Pyatt shifts according to (10). Free electrons are created in ionization processes, and they may leave the system due to outer ionization. This is described by

$$\frac{dN_e}{dt} = \sum_{i=1}^{Z_n} W_{i-1} N_{i-1} - W_{\text{out}} N_e, \quad (30)$$

where N_e is the total number of free electrons and W_{out} denotes the outer ionization rate, for which we use the free streaming

rate of Ditmire *et al.* [5],

$$W_{\text{out}} = \frac{2\sqrt{2\pi} n_e}{\sqrt{m_e k_B T_e}} \exp\left(-\frac{(Q+1)e^2}{Rk_B T_e}\right) \times \begin{cases} \frac{\lambda_e}{4R}(12R^2 - \lambda_e^2), & \lambda_e < R, \\ 4R^2, & \lambda_e \geq R, \end{cases} \quad (31)$$

with the mean free path of the electrons $\lambda_e = \bar{v}/v_{ei}$.

For plasmas in strong static electric fields, the field leads to an increase in the collisional ionization rates, whereas it reduces the rates for recombination [54]. A similar situation occurs in the early phase of the laser-cluster interaction when the laser pulse excites the cluster. At later times, when the laser field is absent, the number density of the free electrons in the cluster has decreased drastically due to the expansion of the system. As shown below, the rates for electron-impact excitation and deexcitation are proportional to n_e , just as the electron-impact ionization rates, (9). In contrast, the rates for the inverse process (three-body recombination) scale proportionally to n_e^2 [45]. Thus, the recombination rates play only a minor role after the laser pulse. As a consequence, following the previous nanoplasma calculations [36,38,39], we neglect recombination in all stages of the laser-cluster interaction. Nevertheless, we want to mention that for clusters excited with XUV pulses at lower intensities, recombination was observed to be responsible for the formation of Rydberg atoms followed by subsequent reionization [55].

G. Numerical results for the ground-state model

Figure 1 shows the ionization dynamics for an argon cluster with initial radius 25 nm and a pulse with wavelength 825 nm, pulse width 130 fs, and laser peak intensity 10^{15} W/cm² [Fig. 1(a)] and 10^{16} W/cm² [Fig. 1(b)]. The initial temperature of the clusters is taken to be 300 K. The total numbers N_i of ions in charge states i are normalized to the number of atoms in the initially neutral cluster, N_a , for which we adopt liquid densities, and $t = 0$ indicates the instant in time when the laser pulse maximum is reached. Before the laser-cluster interaction, only atoms are present in the cluster. In the progress of the laser excitation, free electrons and ions are created, and the heating of the produced nanoplasma leads to a continuing ionization up to high charge states. After the laser pulse, the heating and ionization stop. Then the temperature decreases due to the cluster expansion, and the system “freezes out”, which means that the numbers of ions in the respective charge states remain constant. With increasing peak intensity, the ionization dynamics is accelerated, i.e., shifted to smaller times t . Furthermore, higher charge states are reached at the end of the simulation in the case of more intense laser pulses. A significant peak occurs at the charge state $Z = 8$ due to the stable Ne configuration of the Ar⁸⁺ ion. As a consequence, the ionization energy for the next ionization step is much higher than the ionization energies for smaller Z . Thus, the ionization dynamics is slowed down until the temperature is increased due to the heating of the system, so that the ionization can proceed to higher charge states.

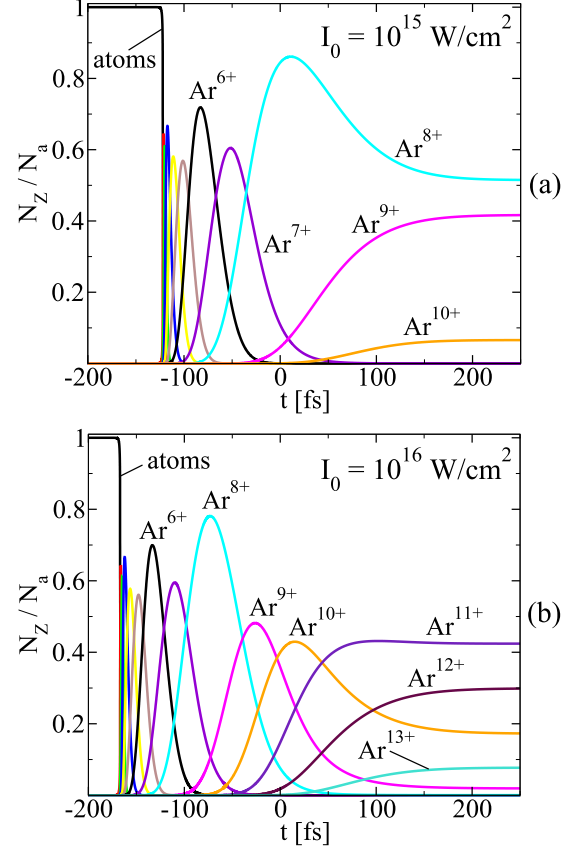


FIG. 1. (Color online) Population of ionic charge states for an argon cluster with initial radius $R_0 = 25$ nm and a laser pulse with wavelength $\lambda = 825$ nm and width $\tau = 130$ fs. The peak intensity is (a) $I_0 = 10^{15}$ W/cm² and (b) $I_0 = 10^{16}$ W/cm².

III. CONSIDERATION OF EXCITED STATES IN THE LASER-CLUSTER INTERACTION

A. Bundling scheme for ground states and excited states

For inclusion of excited states in the nanoplasma model, the energy levels of the atoms and ions as well as the cross sections for excitation and deexcitation between all the different levels must be known for all charge states Z . Because it is numerically not feasible to consider each excited level as an individual particle species in the model, it is not possible to take all transitions between all the different levels into account at each instant during the simulation, and approximations must be made. In MD simulations of dense carbon and Xe-doped hydrogen plasmas [56], the relatively simple bottleneck approximation [57–59] was used. However, this method does not provide detailed information about individual excited states. In [38], the energy levels as well as the excitation rates for the various transitions between states with quantum numbers (n, l, m) and (n', l', m') were bundled for each charge state Z in order to study the ionization dynamics in laser-excited argon clusters. With this procedure, levels with the same n are grouped together assuming that the relative populations of levels in one group are “close to statistical” [38]. However, the atomic and ionic levels in the laser-excited cluster are not in equilibrium, and thus the exact statistical distribution within one charge state Z and quantum number n is not known.

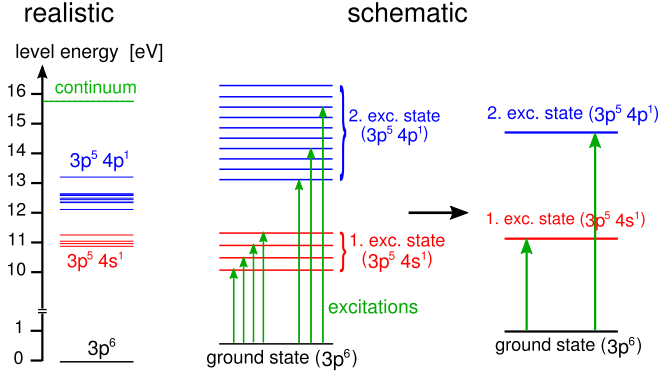


FIG. 2. (Color online) Scheme for the bundling of energy levels to combined states, exemplarily shown for the lowest levels of the argon atom.

In this paper, we distinguish between states with different quantum numbers l and l' . Energy levels with the same fine structure are bundled, and the result is denoted a *state*. Because radiative electric dipole transitions occur between levels with different l 's, this enables us to incorporate photon emission into our model explicitly. For calculation of (i) the energy levels and (ii) the cross sections for transitions between these levels, we use the *Flexible Atomic Code* (FAC) [60] by Gu [61], which was applied, e.g., to model the emission of fusion plasmas [62], to simulate x-ray spectra in laboratory and astrophysical argon plasmas [63], and to analyze laser-excited krypton clusters [64]. In Fig. 2, the simplification scheme for the reduction of a set of energy levels to a smaller number of states is shown exemplarily for the lowest energy levels of the argon atom.

In order to obtain collisional excitation rates for the transition from one state to another, the cross sections for transitions between different levels must be combined. As an example, the excitation cross section for a transition from the ground state to the first excited state of the argon atom is given as

$$\sigma_{\text{exc}}^{(0 \rightarrow 1)} = \sum_{i=1}^4 \sigma_{0 \rightarrow i}, \quad (32)$$

where superscripts denote a state (with 0 corresponding to the ground state, 1 corresponding to the first excited state, etc.), while subscripts denote the energy level (with 0 corresponding to the lowest level). For the transitions between individual energy levels, the cross sections $\sigma_{i \rightarrow j}$ are calculated with the FAC. Cross sections for the transitions between different states are then obtained with the bundling (32). For ground states containing not just one, but several energy levels, the combined cross sections for excitations starting from the different lower levels prove to be nearly identical. This makes it possible to calculate combined excitation cross sections for a transition from state A to state B as

$$\sigma_{\text{exc}}^{(A \rightarrow B)} \approx \sum_{i=B_{\min}}^{B_{\max}} \sigma_{A_{\min} \rightarrow i}, \quad (33)$$

where A_{\min} is the lowest-lying level of state A , and the sum is with respect to the whole state B with energy levels $B_{\min}, B_{\min} + 1, \dots, B_{\max}$.

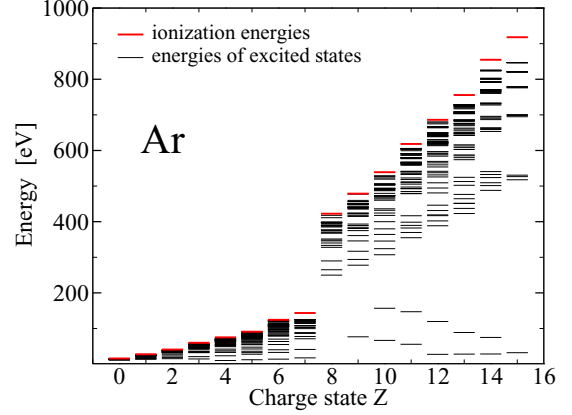


FIG. 3. (Color online) Ionization energies [65] and energies required for excitation from the ground state (calculated with the FAC) for different charge states Z of argon.

In addition to the bundling procedure, we make use of the following simplifications: (i) A maximum principal quantum number $n_{\max} = 7$ is introduced, and all excited states with $n > n_{\max}$ (for which the excitation energy is close to the ionization energy) are neglected. This takes into account approximately that the lowering of the ionization energies leads to the vanishing of the high-lying excited states [46]. (ii) Only those excitation processes in which one electron from the outermost populated atomic shell is shifted to another subshell with the same or a higher n are accounted for. This simplification is justified because the energies required to produce inner-shell excitations are much higher than the energies for excitations from the outermost populated shell, and only a small fraction of the free electrons in the nanoplasma is fast enough to produce inner-shell excitations. (iii) Processes in which two or more free electrons collide with an atom or ion at the same time are neglected, because the probability of such processes is low. (iv) We neglect multiple excitations in which two or more bound electrons are shifted to a higher-lying subshell because the excitation energies required for multiple excitations are typically even higher than the ionization energy. By making use of these simplifications, a total number of 708 particle species is considered in the model: the electrons, 19 ground states ($Z = 0 \dots 18$), and 688 excited atomic or ionic states. The excitation energies—i.e., the energies required for excitation from the ground state—are shown in Fig. 3 together with the ground-state ionization energies for the different charge states of argon up to $Z = 16$. It is shown that the large energy gaps given by the ionization energies [gray (red) lines]—which determine the speed of the ionization dynamics—are significantly reduced via the inclusion of the excited states (black lines).

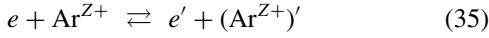
B. Rates for collisional excitation and deexcitation

After fitting the numerical FAC output of the combined cross sections $\sigma_{\text{exc}}^{(l \rightarrow u)}$ for a transition from a lower state (l) to an upper state (u) with appropriate fitting functions, we can obtain analytical results for the collisional excitation rates. For calculation of the electron-impact excitation rates $W_{\text{exc}}^{(l \rightarrow u)}$ from the combined excitation cross sections, the same

procedure can be applied as for the calculation of ionization rates from the ionization cross sections in Sec. II B, and one obtains, analogously to (9),

$$W_{\text{exc}}^{(l \rightarrow u)} = \frac{4n_e k_B T_e}{(2\pi m_e k_B T_e)^{3/2}} \int_0^\pi d\varphi \int_{p_{\min}}^\infty dp_e p_e^2 \sigma_{\text{exc}}^{(l \rightarrow u)}(p_e) \times \frac{\sinh\left(\frac{p_e e E_{\text{int}} \cos \varphi}{\omega m_e k_B T_e}\right)}{\frac{e E_{\text{int}}}{\omega} \cos \varphi} \exp\left\{-\frac{p_e^2 + \frac{e^2 E_{\text{int}}^2}{\omega^2} \cos^2 \varphi}{2m_e k_B T_e}\right\}, \quad (34)$$

where $\Delta E_{\text{exc}}^{(l \rightarrow u)} = E_u - E_l > 0$ is the excitation energy and $p_{\min}^2 = 2m_e \Delta E_{\text{exc}}^{(l \rightarrow u)}$. In the laser-excited cluster, excitation and deexcitation processes of the form



occur, where the left-hand side represents the lower state of the ion and the right-hand side represents the upper state. For the two states and the free electrons e and e' , energy conservation holds,

$$\frac{p_e^2}{2m_e} = \frac{p_e'^2}{2m_e} + \Delta E_{\text{exc}}^{(l \rightarrow u)}, \quad (36)$$

with p_e and p_e' being the momenta of the electron. Technically, the rates for deexcitation due to electron impact, $W_{\text{deexc}}^{(u \rightarrow l)}$, can be written similarly to the rates for ionization and excitation in terms of a deexcitation cross section $\sigma_{\text{deexc}}^{(u \rightarrow l)}$ [compare Eq. (8)]:

$$W_{\text{deexc}}^{(u \rightarrow l)} = \frac{n_e}{T} \int_0^T dt \int d^3 p_e' f(\mathbf{p}_e' - \mathbf{p}_{\text{os}}(t)) \frac{p_e'}{m_e} \sigma_{\text{deexc}}^{(u \rightarrow l)}(p_e'). \quad (37)$$

In the nanoplasma model, an equilibrium distribution function for the electrons can always be applied. Moreover, the Klein-Rosseland relation [41,66]

$$g_l p_e^2 \sigma_{\text{exc}}^{(l \rightarrow u)}(p_e) = g_u p_e'^2 \sigma_{\text{deexc}}^{(u \rightarrow l)}(p_e') \quad (38)$$

holds, with g_l and g_u being the statistical weights of the lower and upper state, respectively. By inserting (38) into (37) and carrying the integration out partly analytically, one obtains

$$W_{\text{deexc}}^{(u \rightarrow l)} = \frac{g_l}{g_u} \frac{4n_e k_B T_e}{(2\pi m_e k_B T_e)^{3/2}} \int_0^\pi d\varphi \int_0^\infty dp_e' p_e'^2 \sigma_{\text{exc}}^{(l \rightarrow u)}(p_e') \times \frac{\sinh\left(\frac{p_e' e E_{\text{int}} \cos \varphi}{\omega m_e k_B T_e}\right)}{\frac{e E_{\text{int}}}{\omega} \cos \varphi} \exp\left\{-\frac{p_e'^2 + \frac{e^2 E_{\text{int}}^2}{\omega^2} \cos^2 \varphi}{2m_e k_B T_e}\right\}, \quad (39)$$

with p_e given from (36). In the limit of a vanishing laser field, the rates for excitation and deexcitation can be simplified. Then they are connected by the usual detailed balance relation [41],

$$W_{\text{deexc}}^{(u \rightarrow l)} = \frac{g_l}{g_u} W_{\text{exc}}^{(l \rightarrow u)} \exp\left\{\frac{\Delta E_{\text{exc}}^{(l \rightarrow u)}}{k_B T_e}\right\}. \quad (40)$$

C. Modified equation for the temperature

Because free electrons lose energy to heavy particles in collisional excitations and they gain energy from atoms or

ions in collisional deexcitation processes, the terms

$$-\sum_{l,u} \Delta E_{\text{exc}}^{(l \rightarrow u)} \frac{dN_u}{dt} \Big|_{\text{excitation}, l \rightarrow u} + \sum_{l,u} \Delta E_{\text{exc}}^{(l \rightarrow u)} \frac{dN_l}{dt} \Big|_{\text{deexcitation}, u \rightarrow l} \quad (41)$$

must be added in Eq. (17), describing the temporal change of the electrons' internal energy. Consequently, Eq. (20), determining the temperature evolution, becomes

$$\frac{\partial T_e}{\partial t} = -\frac{2T_e}{R} \frac{dR}{dt} + \frac{1}{C} \left\{ \dot{U}_{\text{laser}} - \sum_j \frac{dN_j}{dt} \Big|_{\text{ionization}} \times \left(\frac{3}{2} k_B T_e + I_{\text{ion}}^{(j)} - \Delta E_{\text{SP}}^{(j)} \right) - \sum_{l,u} \Delta E_{\text{exc}}^{(l \rightarrow u)} \frac{dN_u}{dt} \Big|_{\text{excitation}, l \rightarrow u} + \sum_{l,u} \Delta E_{\text{exc}}^{(l \rightarrow u)} \frac{dN_l}{dt} \Big|_{\text{deexcitation}, u \rightarrow l} \right\}. \quad (42)$$

It should be noted that the dense plasma not only lowers the ionization energies, but also affects the excitation energies. However, because this effect shows a weaker density dependence [46], it is neglected here.

D. Numerical results for single-pulse excitation

To account for excitation and deexcitation processes, the stepwise inclusion of excited states in the nanoplasma model was carried out. Starting for each charge state Z with excitation from the ground state to all excited states (and including the inverse deexcitation processes), we then added the excitation from the first excited state to the higher excited states and proceeded in this manner until a convergence in the ionization dynamics was reached. The processes thus included in our extended model are summarized in Fig. 4. To investigate the effect stemming from the inclusion of excited states, the ionization dynamics of an argon cluster is shown in Fig. 5

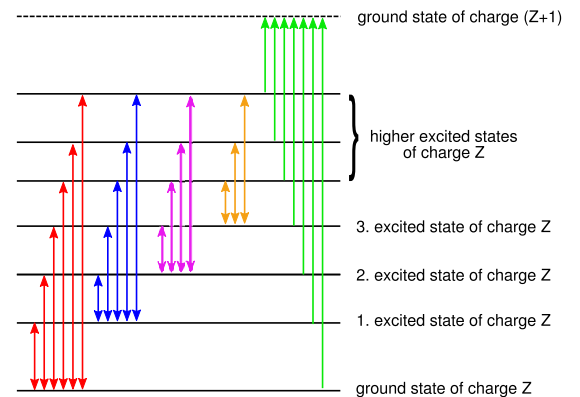


FIG. 4. (Color online) Scheme of the excitation processes, deexcitation processes, and ionization processes included in the extended nanoplasma model.

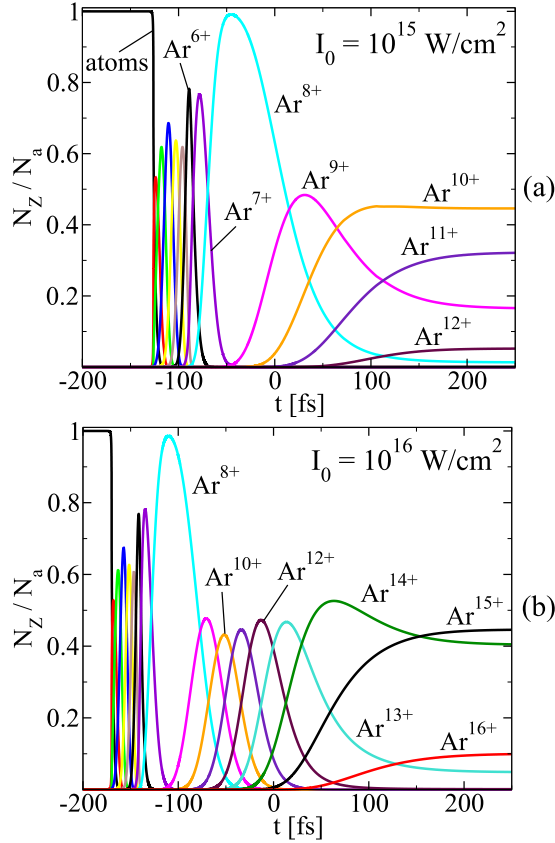


FIG. 5. (Color online) Population of ionic charge states for the same parameters as in Fig. 1. Ground states and excited states are considered in the simulation for the peak intensity: (a) $I_0 = 10^{15}$ W/cm² and (b) $I_0 = 10^{16}$ W/cm².

for the same parameters as in Fig. 1 for the ground-state model. Compared to the ground-state model, the inclusion of excited states leads to accelerated ionization dynamics, in particular for high peak intensities [compare Figs. 1(b) and 5(b)]. Therefore, higher charge states up to $Z = 16$ are reached at the end of the laser-cluster interaction with the extended model. In the ground-state model, the peak at charge state $Z = 8$ is due to the large energy gap in the ionization energies resulting from the stable noble-gas configuration of the Ar^{8+} ion. In the extended model including excited states, the peak at $Z = 8$ is due to an energy gap in the excitation energies: The Ar^{8+} ground state can be reached quite rapidly via processes requiring only low excitation or ionization energies (compare Fig. 3). But for excitation from the Ar^{8+} ground state to excited states, considerably more energy is needed. Thus, the system must be heated up first so that a significant fraction of the free electrons is fast enough to produce the further excitation. Therefore, the ionization dynamics is slowed down, leading to the Ar^{8+} peak in Fig. 5.

In Fig. 6, results are presented for the temporal evolution of the electron temperature T_e [Fig. 6(a)] and the number density n_e of the electrons normalized to the critical density n_{crit} at which the laser frequency matches the plasma frequency [Fig. 6(b)]. Two values of the peak intensity are considered, $I_0 = 10^{15}$ W/cm² (black curves) and $I_0 = 10^{16}$ W/cm² (red curves); the other parameters are as in Fig. 1. Dashed

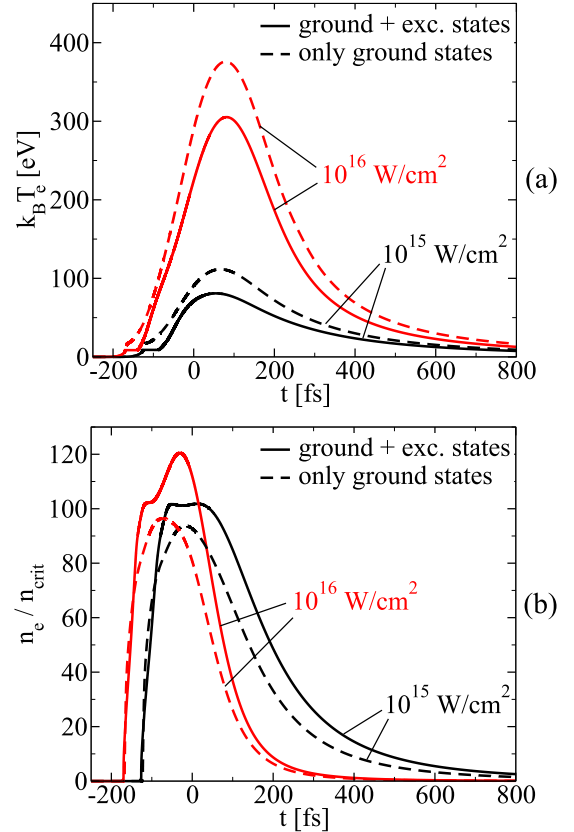


FIG. 6. (Color online) (a) Electron temperature and (b) number density of electrons as a function of time for an argon cluster with initial radius $R_0 = 25$ nm. Different values of the peak intensity I_0 are considered for a laser pulse with wavelength $\lambda = 825$ nm and pulse width $\tau = 130$ fs.

curves indicate the results from the ground-state model, while solid curves represent the results from the extended model including excited states. In the case of the higher intensity, more energy is transferred into the cluster. This results in a stronger heating and thus a higher temperature [see Fig. 6(a)] and in a faster expansion accompanied by a faster decrease in the electron density compared to the case for the lower intensity [see Fig. 6(b)]. The inclusion of excited states leads to a decrease in the electron temperature [compare the dashed and solid curves in Fig. 6(a)]. This is because the free electrons in the nanoplasmalose energy not just in direct ionization processes, but also in excitation processes, which happen earlier. As a result, in the early phase of the laser-cluster interaction almost all energy deposited by the laser field is spent in excitation processes, and the electron temperature shows a plateau at $t \sim -100$ fs for the extended nanoplasmal model (solid curves). The total amount of laser energy absorbed by the cluster can be obtained by integrating the heating term, (23), over time. Comparing this total energy for both models, we find that the inclusion of excited states reduces this energy by $\sim 23\%$ for the peak intensity 10^{16} W/cm² and by $\sim 35\%$ for $I_0 = 10^{15}$ W/cm², which is consistent with the respective temperature reduction shown in Fig. 6(a). Due to the enhanced ionization dynamics, the number density of free electrons in the cluster is increased if excited states are taken

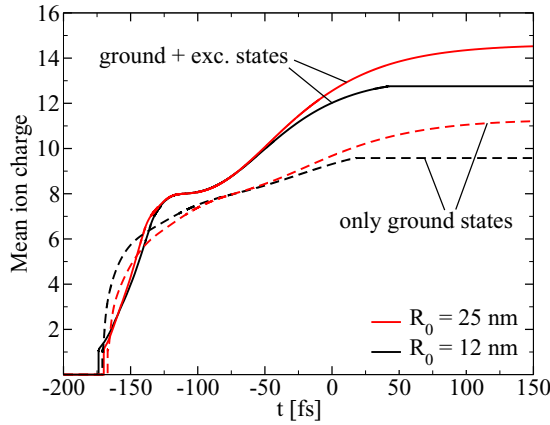


FIG. 7. (Color online) Mean ion charge as a function of time for a laser pulse with pulse width $\tau = 130$ fs, peak intensity $I_0 = 10^{16}$ W/cm², and wavelength $\lambda = 825$ nm. Different values of the initial cluster radius R_0 are considered.

into account [compare the solid and dashed curves in Fig. 6(b)]. In the extended model, a plateau can be observed, which is related to the Ar^{8+} peak in the ionization dynamics discussed above.

In Fig. 7, the mean ionic charge state is shown as a function of time for a smaller cluster with $R_0 = 12$ nm and a larger cluster with $R_0 = 25$ nm, which correspond to particle numbers of 1.5×10^5 and 1.4×10^6 cluster atoms, respectively. A laser pulse with $\lambda = 825$ nm, pulse width $\tau = 130$ fs, and peak intensity $I_0 = 10^{16}$ W/cm² is considered, and again, results for the ground-state model (dashed curves) are compared with results for the extended model (solid curves). It is shown that for the larger cluster, a higher mean ionic charge state is reached at the end of the simulation. Moreover, the consideration of excited states increases the final mean charge state by approximately 1.5 units, independent of the initial radius R_0 . The fact that the production of high charge states is favored for larger clusters is due to the qualitatively different cluster evolution in the case of smaller clusters. This is shown in Fig. 8, in which the Gaussian external laser field is shown together with the internal field inside the cluster. For the same laser parameters as in Fig. 7, clusters with $R_0 = 20$ nm and $R_0 = 25$ nm are considered, which corresponds roughly to a doubling of the cluster volume. In the beginning of the laser-cluster interaction, the internal field matches the external laser field until the Mie resonance is reached at $t \sim -170$ fs, where the internal field is increased. In the subsequent cluster evolution, the external field is screened, and thus the internal field is drastically diminished. For the smaller cluster, a second Mie resonance develops at the rear side of the laser pulse, leading to an additional rise of the internal field. In the second Mie resonance, more laser energy is absorbed by the system. Consequently, the electron temperature (presented in Fig. 9) shows a pronounced peak in the case of the smaller cluster. The reason for the second Mie resonance is the faster cluster expansion. As a result, the electron density drops down more rapidly so that the resonance condition is fulfilled a second time. It should be noted that although the smaller cluster is heated more strongly, higher charge states are reached for the larger

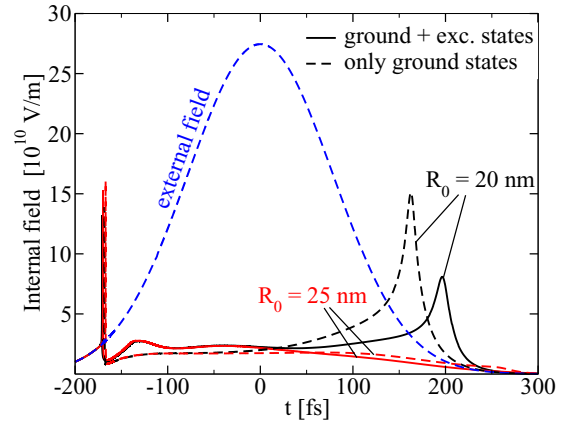


FIG. 8. (Color online) External laser field and internal field inside the cluster for a pulse with wavelength $\lambda = 825$ nm, pulse width $\tau = 130$ fs, and peak intensity $I_0 = 10^{16}$ W/cm². Different values of the initial cluster radius R_0 are considered.

cluster. This is because the rates for collisional excitation and ionization scale with the electron density. As a consequence, if the system expands too rapidly, ionization stops earlier.

E. The role of deexcitation processes

It was shown by Micheau *et al.* [38] that the inclusion of excitation processes leads to accelerated ionization dynamics and thus to the creation of higher ionic charge states. As discussed in the previous section, this is confirmed by our simulations. To investigate the relevance of deexcitation processes, we compare in this section (i) numerical results from the nanoplasma model, where the deexcitation processes are neglected, and (ii) results from the “full” model, in which deexcitation is included. Concerning the ionization dynamics, this comparison is made by means of Fig. 10, which shows the ionization dynamics for the same parameters as in Fig. 5(a), but neglecting deexcitation processes. Without deexcitation (Fig. 10) the Ar^{8+} peak is reached earlier. Aside from this, the overall behavior of the ionization dynamics is the same as in Fig. 5(a). The consideration of deexcitation processes in Fig. 5(a) leads to only a small reduction in the mean charge

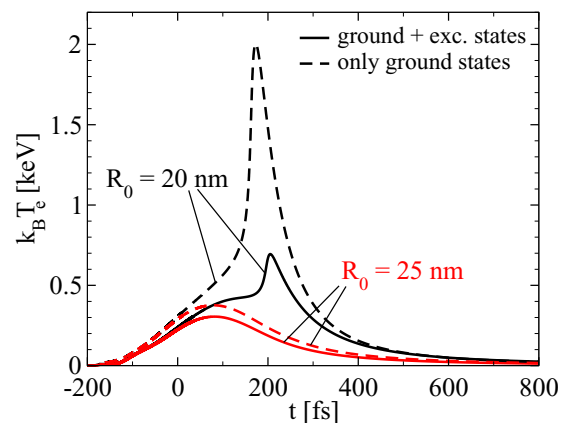


FIG. 9. (Color online) Electron temperature as a function of time for the same parameters as in Fig. 8.

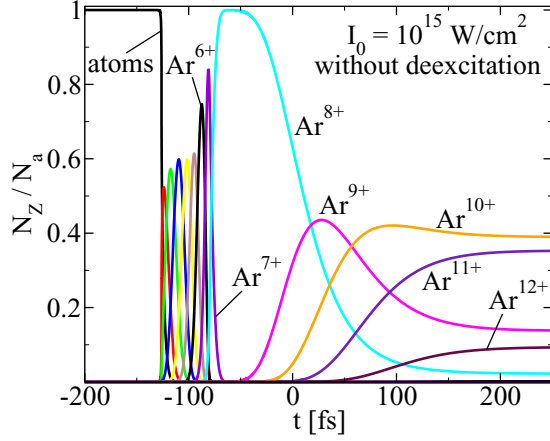


FIG. 10. (Color online) Population of ionic charge states for the same parameters as in Fig. 5(a). Deexcitation processes were neglected in the simulation.

state reached at the end of the simulation, which is $\bar{Z} = 10.37$ if deexcitation is neglected and $\bar{Z} = 10.24$ if deexcitation processes are included. This means that regarding the temporal evolution of the ionic charge states only, the incorporation of

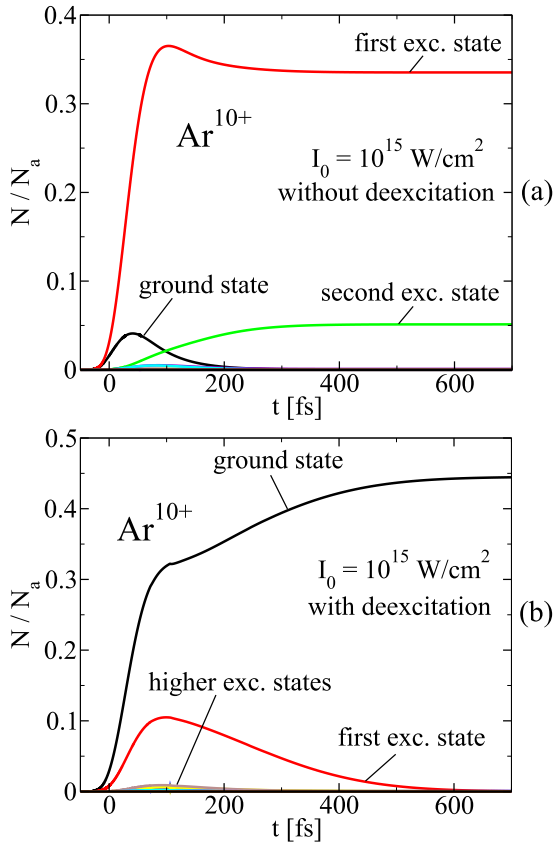


FIG. 11. (Color online) Population of ground states and excited states of Ar^{10+} for an argon cluster with initial radius $R_0 = 25$ nm and a laser pulse with wavelength $\lambda = 825$ nm, pulse width $\tau = 130$ fs, and peak intensity $I_0 = 10^{15}$ W/cm² when (a) deexcitation processes are neglected and (b) deexcitation processes are included.

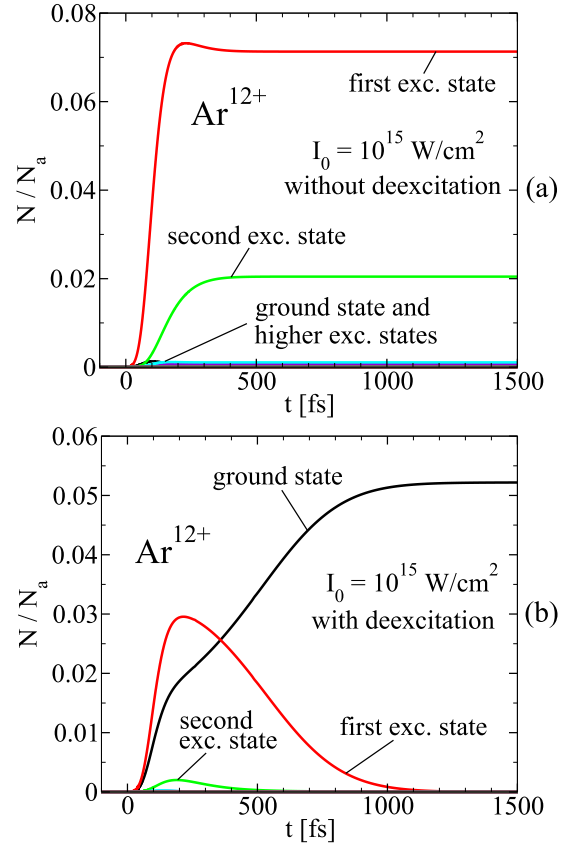


FIG. 12. (Color online) Population of ground states and excited states of Ar^{12+} ions for the same parameters as in Fig. 11 when (a) deexcitation processes are neglected and (b) deexcitation processes are included.

deexcitation processes in the nanoplasma model has only a small effect.

However, because each charge state shown in Figs. 5(a) and 10 contains particles in the ground state and particles in excited states as well, we want to examine the population of ground states and excited states for ions with the same charge in detail. For this purpose, the population of ground states and excited states is presented for Ar^{10+} and Ar^{12+} ions in Figs. 11 and 12 for the same laser and cluster parameters as in Fig. 10. If deexcitation processes are neglected [Figs. 11(a) and 12(a)], ions in excited states cannot return to the ground state. They can either be shifted to higher excited states or become ionized. Consequently, many ions remain in excited states at the end of the laser-cluster interaction. In contrast, if collisional deexcitation is taken into account [Figs. 11(b) and 12(b)], excited ions can return to the ground state. As a result, only ground states are populated for $t \rightarrow \infty$ in Figs. 11(b) and 12(b). This means that the consideration of deexcitation processes significantly changes the population within one charge state Z .

For a stronger laser pulse with $I_0 = 10^{16}$ W/cm² (the other parameters are unchanged), the population of ground states and excited states—obtained with the complete model including deexcitation—is shown for charge state $Z = 15$ in Fig. 13. Due to the stronger pulse, there is faster cluster expansion, and the system freezes out before all excited ions can return to the

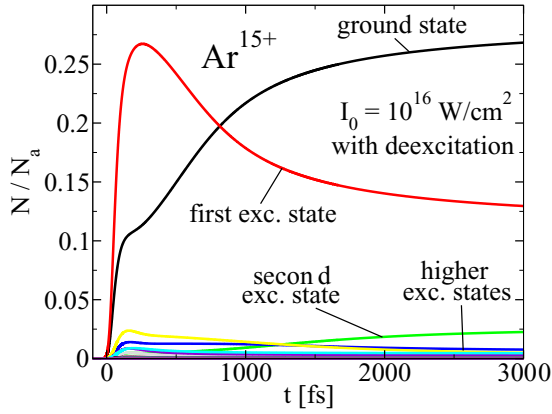


FIG. 13. (Color online) Population of ground states and excited states of Ar^{15+} ions when deexcitation processes are included for an argon cluster with initial radius $R_0 = 25$ nm and a laser pulse with wavelength $\lambda = 825$ nm, pulse width $\tau = 130$ fs, and peak intensity $I_0 = 10^{16}$ W/cm 2 .

ground state via collisional deexcitation. Therefore, at the end of the laser-cluster interaction particles remain in excited states for which radiative transitions can be observed (see below).

F. Double-pulse excitation

By using excitation schemes more sophisticated than single-pulse excitation, the yield of ions with a certain charge can be enhanced. In experiments, an optimized yield of silver ions was found by shaping the amplitude and phase of tailored laser pulses [67], where the optimized pulse shape appeared to be a simple double-pulse structure. Such a structure was also found numerically with the nanoplasma model of Hilse *et al.*, investigating laser-excited silver and xenon clusters [67–69]. Because excited states were neglected in these previous works, it is interesting to see how the consideration of excited states in our extended model modifies the ion yield resulting from double-pulse excitation. For this purpose, we consider argon clusters irradiated with IR laser radiation whose time-dependent intensity is given as a superposition of two Gaussians,

$$I(t) = I_1 \exp\left\{-\frac{4 \ln 2}{\tau_1^2} t^2\right\} + I_2 \exp\left\{-\frac{4 \ln 2}{\tau_2^2} (t - \Delta t)^2\right\}, \quad (43)$$

where I_i is the peak intensity of the i th pulse ($i = 1, 2$), τ_i is the pulse width, and Δt is the delay time between the two pulses. In Fig. 14, the yield of Ar^{13+} ions reached at the end of the laser-cluster simulation is shown as a function of the delay time for a double-pulse excitation with $\tau_1 = \tau_2 = 130$ fs and an initial cluster radius $R_0 = 25$ nm. Results are presented for the ground-state model neglecting excited states in Fig. 14(a) and for the extended model in which excited states are included in Fig. 14(b). Under the constraint that $\int_{-\infty}^{\infty} dt I(t) = \text{const.}$, the ratio I_1/I_2 of the peak intensities was varied, corresponding to a single pulse with peak intensity 2×10^{15} W/cm 2 .

It is shown in Fig. 14(a) that for every ratio of the peak intensities, there exists a certain delay time for which the ion yield is maximized. At this optimal delay time, the second

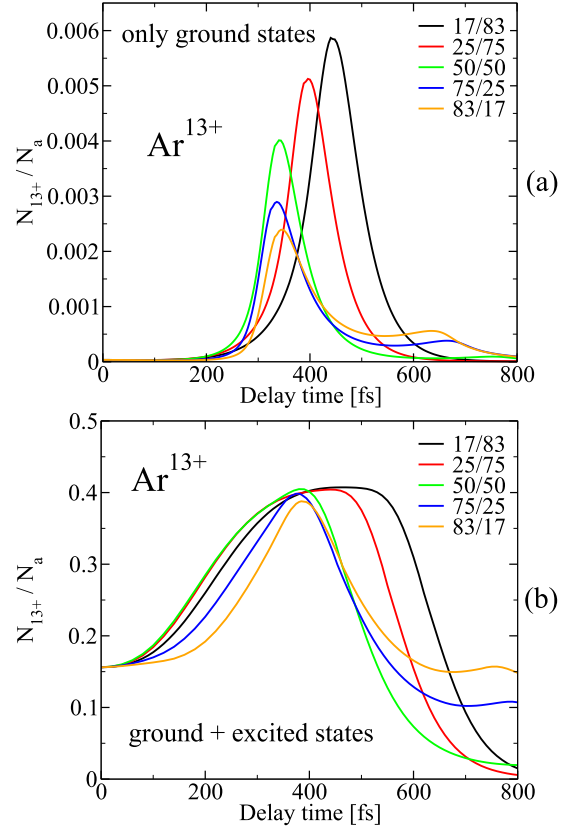


FIG. 14. (Color online) Yield of Ar^{13+} ions from double-pulse excitation as a function of the delay time between the pulses. Different ratios I_1/I_2 of the peak intensities are considered for laser pulses with pulse width $\tau_1 = \tau_2 = 130$ fs and a cluster with initial radius $R_0 = 25$ nm. (a) Only ground states were taken into account in the simulation. (b) Ground states and excited states were included in the simulation.

laser pulse hits the cluster just when the condition for the Mie resonance is fulfilled a second time. As a consequence, the amount of energy absorbed by the cluster is enhanced significantly and thus more ions with high charge states are produced. The maximum of the ion yield is increased and shifted to larger delay times if the ratio of the peak intensities is decreased. This means that, in order to optimize the ion yield, it is advantageous to use a smaller prepulse followed by a larger main pulse, thus reproducing the optimized double-pulse characteristics known from silver clusters [67,69]. If excited states are included, the behavior is qualitatively similar. However, by taking excited states into account, more Ar^{13+} ions are produced. In addition, the pronounced peak of the ion yield appearing in the ground-state model in Fig. 14(a) is flattened, and the region of “optimal” delay times is broadened if excited states are taken into account [see Fig. 14(b)]. This broader behavior was also observed in optimization experiments [70].

IV. EMISSION OF RADIATION

A. Preliminary considerations

An important feature observed in the interaction of laser pulses with atomic clusters is light emission in the ultraviolet

regime and the adjacent soft x-ray regime. Here we restrict our investigations to electric dipole radiation, which gives the largest contribution. Typically, photon emission with energies up to several hundred electron volts is produced as follows: In the first step, a bound electron from the outermost populated shell of a highly charged ion is shifted to a higher-lying shell in an excitation process. Afterwards, the electron can return to the lower-lying shell via spontaneous photon emission. In contrast, emission in the kilo-electron-volt regime typically originates from inner-shell excitations producing a K -shell vacancy. When a bound electron from an outer shell fills the vacancy, energetic x-ray photons are emitted. Because radiative transitions occur between different energy levels belonging to different bundled states, an assumption is needed about how the energy levels are populated within a certain state. At thermodynamic equilibrium, the population between levels is balanced according to a Boltzmann distribution [41],

$$\frac{N_i}{N_j} = \frac{g_i}{g_j} \exp\left(-\frac{\Delta E_{ij}}{k_B T_e}\right), \quad (44)$$

where N_i is the number of ions with level energy E_i , g_i is the statistical weight of the level, and $\Delta E_{ij} = E_i - E_j > 0$. Within one combined state, we assume (44) to be valid. Because the energy levels E_i and E_j within the same combined state are very close, one finds that $\Delta E_{ij} \ll k_B T_e$, and the population of an individual level within a state is approximately given as

$$N_i = \frac{g_i}{g_{\text{tot}}} N_{\text{tot}}, \quad (45)$$

where $N_{\text{tot}} = \sum_i N_i$ is the number of particles in the bundled state, which is calculated for every ground state and every excited state at each instant during the simulation, and $g_{\text{tot}} = \sum_i g_i$ is the statistical weight of the state. Although the temperature decreases strongly at the end of the laser-cluster interaction due to the expansion of the system, one can still assume (45) to be valid: because the electron density also drops down rapidly during the cluster expansion, there are no more collisions of the ions with free electrons. Therefore, no more collisional excitation or deexcitation processes can occur, and the population of levels given by (45) just “freezes out”. The number of photons emitted from the transition $i \rightarrow j$ (levels i and j belonging to different states), $N_{i \rightarrow j}^\gamma(t)$, can be obtained at each instant in time by multiplying the respective level population $N_i(t)$ by the corresponding radiative decay rate $W_{i \rightarrow j}^\gamma$, which we also calculated with the FAC:

$$N_{i \rightarrow j}^\gamma(t) = W_{i \rightarrow j}^\gamma N_i(t) dt. \quad (46)$$

The total photon yield from the transition $i \rightarrow j$ in the laser-cluster interaction is then obtained by integrating (46) in the range $-\infty > t > \infty$.

B. Emission from the excitation of outer-shell electrons

In a dense nanoplasma, the spontaneous emission rates for radiative transitions involving only outer ionic shells are orders of magnitudes smaller than the rates for collision-induced transitions, because the latter scale with the electron density. As a consequence, radiative transitions become important only after the laser pulse when the density has strongly decreased

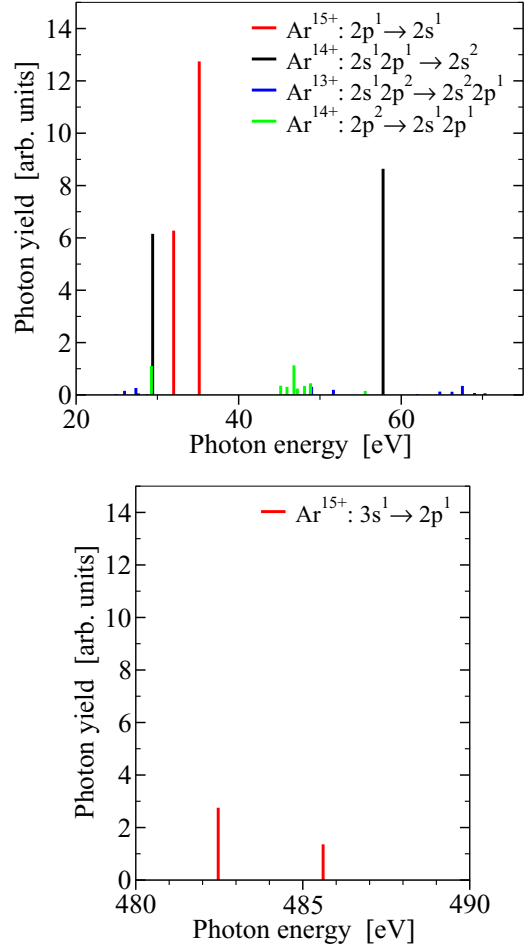


FIG. 15. (Color online) Calculated photon yield from different charge states Ar^{Z+} for a cluster with initial radius $R_0 = 25$ nm and a laser pulse with $\lambda = 825$ nm, pulse width $\tau = 130$ fs, and peak intensity $I_0 = 10^{16}$ W/cm². For each charge state, transitions are considered from the first excited state to the ground state and from the second excited state to the first excited state.

due to the expansion of the system and collisions become negligible, and thus the photon yield is determined by the population of excited states at the end of the laser-cluster interaction. For the parameters considered in Fig. 13, the cluster expands rapidly enough so that for $t \rightarrow \infty$, not only the ground state, but also the two lowest excited states show a significant population. The resulting photon yield, originating from highly charged ions present after the laser pulse, is shown in Fig. 15. Depending on the charge state, the respective transitions are either from levels belonging to the first excited state to ground-state levels or from levels belonging to the second excited state to levels bundled in the first excited state. A significant emission is obtained for two transitions at higher energies, ~ 485 eV. Moreover, photon emission is observed at lower energies, between 20 and 75 eV. In Fig. 15, only photons resulting from transitions of high charge states $Z \geq 13$ are shown, because the lower charge states are not populated at the end of the laser pulse. Moreover, no emission resulting from transitions of Ar^{16+} is shown in Fig. 15 because the

related photon energies are in the kilo-electron-volt regime, which is considered below.

C. Emission from inner-shell excitations

Finally, we want to refer to theoretical and experimental results presented in [38,71], where the spectrum of emitted photons with energies of several keV was measured for a larger cluster with initial radius $R_0 = 35$ nm and a laser pulse with width $\tau = 500$ fs and peak intensity $I_0 = 1.6 \times 10^{16}$ W/cm². Typically, $K\alpha$ lines originating from $2p \rightarrow 1s$ (electric dipole) transitions are associated with such energetic photons. The respective emission occurs either from Ar^{16+} transitions involving the outermost bound electron or from ions with charge states $Z \leq 15$ due to transitions involving a K -shell vacancy. The relevant excited state of Ar^{16+} is already included in the extended nanoplasma model, and the states with a K -shell vacancy can be introduced into the model as new particle species in exactly the same manner as the other excited states. We assume that these states are created via collisional excitation from the ground state, from the first excited state, or from the second excited state. Moreover, it is assumed that they are destroyed in one of the following processes: (i) collisional deexcitation to the ground state, to the first excited state, or to the second excited state; (ii) spontaneous radiative transitions to the ground state, to the first excited state, or to the second excited state—this depends on the specific transition—via x-ray emission; or (iii) Auger decay via electron emission, where we assume that the final state of an Auger-decayed ion is the ground state of the next-higher charge state. The rates for collisional excitation and deexcitation as well as the radiative transition rates were calculated with the FAC, whereas the rates for Auger decay were taken from [72].

In Fig. 16, the measured x-ray spectrum from [38] is shown [(blue) curve]. The spectrum contains different peaks, which are related to the $K\alpha$ lines of the charge states $Z = 13 \dots 16$ [38]. This measured spectrum is compared to the x-ray yield for the different charge states of argon ions calculated with the nanoplasma model of Micheau *et al.*

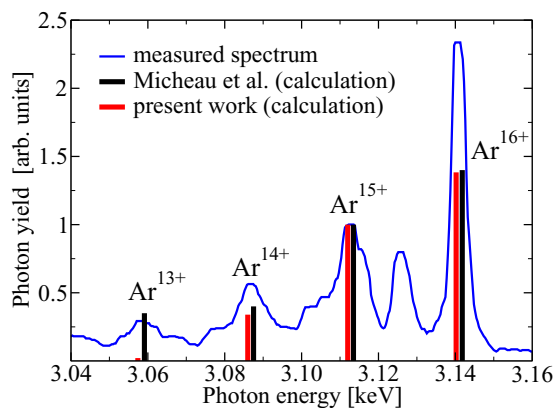


FIG. 16. (Color online) Calculated photon yield from different charge states of highly charged argon ions in different models and measured x-ray spectrum from [38] for argon clusters with initial radius $R_0 = 35$ nm and laser pulses with peak intensity $I_0 = 1.6 \times 10^{16}$ W/cm² and pulse width $\tau = 500$ fs.

(black vertical bars) and with our extended model [gray (red) vertical bars]. The results were normalized so that the calculated photon yield for $Z = 15$ equals the intensity of the corresponding measured peak. Please note that the peak at the energy ~ 3.125 keV in Fig. 16 corresponds to an intercombination line whose transitions were not included in the calculations, and thus, there is no simulated counterpart for this peak. Taking into account the differences between the two computational models—e.g., the fact that deexcitation and the lowering of the ionization energies are both neglected in [38]—the calculated photon yield is quite similar [compare gray (red) and black vertical bars]. The main difference appears for the charge state $Z = 13$. This is because in our model, a higher mean charge state, $\bar{Z} = 15.1$ (compared to $\bar{Z} = 14.7$ in [38]), was obtained at the end of the laser pulse, with only a very small fraction of Ar^{13+} ions remaining. Compared to the measured spectrum, the calculated photon yield shows the same qualitative behavior, namely, an increasing number of photons for $K\alpha$ lines belonging to increasing charge states. However, the simulations cannot fully reproduce the experimental results: aside from the Ar^{13+} yield just discussed, which strongly depends on the computational model, the photon yield for Ar^{16+} , in particular, is underestimated in both theoretical calculations.

V. CONCLUSION

We have investigated the interaction of nanometer-sized argon clusters with femtosecond laser pulses in the IR regime by means of a nanoplasma model. For clusters with initial radii $12 \leq R_0 \leq 35$ nm, the temporal evolution of different plasma parameters was simulated including the number density of the free electrons, the electron temperature, and the population of different ionic charge states. Special emphasis was placed on the effects stemming from the consideration of excitation and deexcitation processes, which are important in order to correctly describe the population of excited states and the associated photon emission. By taking these processes into account in an extended nanoplasma model, we calculated the photon yield from laser-excited clusters.

After introducing the different physical processes of the model and their theoretical descriptions—such as tunnel and collisional ionization and the lowering of the ionization energies, the heating, and the expansion of the cluster—numerical results for the ionization dynamics were discussed in the case of the ground-state model, in which excited states were neglected.

In the second step, excited states were incorporated in the model. To this purpose, individual energy levels were bundled into combined states within a simplified level scheme. Excitation cross sections were calculated with the FAC and collisional excitation rates were found via averaging with respect to the electron distribution function and over one laser cycle, whereas the rates for collisional deexcitation were obtained by means of a relation between excitation and deexcitation cross sections. It was found that with the inclusion of excited states, the ionization dynamics is accelerated, and higher ionic charge states are reached at the end of the laser-cluster interaction. The incorporation of excited states

leads to a reduction of the electron temperature because the free electrons lose energy in excitation processes. Moreover, the free electron density is increased due to the enhanced ionization dynamics. For smaller clusters, a second Mie resonance is observed, resulting in a larger heating and a faster expansion. The population of ionic charge states is only slightly modified by deexcitation processes. However, these processes play an important role for the population of ground states and excited states, which in turn significantly determines the emission of radiation from laser-excited clusters.

Within a double-pulse excitation scheme, maximization of a certain ion yield was found to appear at a certain delay time in the case of a smaller prepulse followed by a larger main pulse. Here the inclusion of excited states resulted in a flattening of the curves; i.e., the region of “optimal” delay

times was broadened. By assuming a Boltzmann distribution for the individual levels within the combined states, the emission of radiation was investigated. The photon yield from the excitation of outer-shell electrons was computed, and by introducing additional particle species with a K -shell vacancy, also the emission from inner-shell excitations was considered, showing a qualitatively good agreement with other theoretical as well as experimental results.

ACKNOWLEDGMENTS

This work was supported by the Deutsche Forschungsgemeinschaft within Sonderforschungsbereich 652. One of the authors (V.P.K.) thanks the Ministry of Education and Science of the Russian Federation (State Assignment No. 3.679.2014/K) for support.

-
- [1] A. McPherson, B. D. Thompson, A. B. Borisov, K. Boyer, and C. K. Rhodes, *Nature* **370**, 631 (1994).
 - [2] T. Ditmire, T. Donnelly, R. W. Falcone, and M. D. Perry, *Phys. Rev. Lett.* **75**, 3122 (1995).
 - [3] T. D. Donnelly, T. Ditmire, K. Neuman, M. D. Perry, and R. W. Falcone, *Phys. Rev. Lett.* **76**, 2472 (1996).
 - [4] J. W. G. Tisch *et al.*, *J. Phys. B: At. Mol. Opt. Phys.* **30**, L709 (1997).
 - [5] T. Ditmire, T. Donnelly, A. M. Rubenchik, R. W. Falcone, and M. D. Perry, *Phys. Rev. A* **53**, 3379 (1996).
 - [6] E. M. Snyder, S. A. Buzza, and A. W. Castelman, Jr., *Phys. Rev. Lett.* **77**, 3347 (1996).
 - [7] Y. L. Shao *et al.*, *Phys. Rev. Lett.* **77**, 3343 (1996).
 - [8] L. M. Chen *et al.*, *Phys. Plasmas* **9**, 3595 (2002).
 - [9] E. Springate, S. A. Aseyev, S. Zamith, and M. J. J. Vrakking, *Phys. Rev. A* **68**, 053201 (2003).
 - [10] V. P. Krainov and M. B. Smirnov, *Phys. Rep.* **370**, 237 (2002).
 - [11] U. Saalmann, C. Siedschlag, and J. M. Rost, *J. Phys. B: At. Mol. Opt. Phys.* **39**, R39 (2006).
 - [12] Th. Fennel *et al.*, *Rev. Mod. Phys.* **82**, 1793 (2010).
 - [13] H. Wabnitz *et al.*, *Nature* **420**, 482 (2002).
 - [14] C. Bostedt *et al.*, *Phys. Rev. Lett.* **100**, 133401 (2008).
 - [15] H. Thomas *et al.*, *Phys. Rev. Lett.* **108**, 133401 (2012).
 - [16] T. Gorkhover *et al.*, *Phys. Rev. Lett.* **108**, 245005 (2012).
 - [17] B. Rudek *et al.*, *Phys. Rev. A* **87**, 023413 (2013).
 - [18] B. Rudek *et al.*, *Nature Photon.* **6**, 858 (2012).
 - [19] U. Saalmann and J.-M. Rost, *Phys. Rev. Lett.* **91**, 223401 (2003).
 - [20] M. Moll, P. Hilse, M. Schlanges, Th. Bornath, and V. P. Krainov, *J. Phys. B: At. Mol. Opt. Phys.* **43**, 135103 (2010).
 - [21] M. Moll, Th. Bornath, M. Schlanges, and V. P. Krainov, *Phys. Plasmas* **19**, 033303 (2012).
 - [22] M. Moll, M. Schlanges, Th. Bornath, and V. P. Krainov, *New J. Phys.* **14**, 065010 (2012).
 - [23] K. Ishikawa and T. Blenski, *Phys. Rev. A* **62**, 063204 (2000).
 - [24] I. Last and J. Jortner, *J. Chem. Phys.* **120**, 1348 (2004).
 - [25] C. Jungreuthmayer, L. Ramunno, J. Zanghellini, and Th. Brabec, *J. Phys. B: At. Mol. Opt. Phys.* **38**, 3029 (2005).
 - [26] Th. Fennel, L. Ramunno, and Th. Brabec, *Phys. Rev. Lett.* **99**, 233401 (2007).
 - [27] M. Arbeiter, C. Peltz, and Th. Fennel, *Phys. Rev. A* **89**, 043428 (2014).
 - [28] I. Georgescu, U. Saalmann, and J. M. Rost, *Phys. Rev. A* **76**, 043203 (2007).
 - [29] T. Taguchi, T. M. Antonsen, Jr., and H. M. Milchberg, *Phys. Rev. Lett.* **92**, 205003 (2004).
 - [30] T. Taguchi, T. M. Antonsen, Jr., J. Palastro, H. Milchberg, and K. Mima, *Opt. Express* **18**, 2389 (2010).
 - [31] M. Kundu, P. K. Kaw, and D. Bauer, *Phys. Rev. A* **85**, 023202 (2012).
 - [32] C. Jungreuthmayer, M. Geissler, J. Zanghellini, and Th. Brabec, *Phys. Rev. Lett.* **92**, 133401 (2004).
 - [33] C. Varin, C. Peltz, Th. Brabec, and Th. Fennel, *Ann. Phys. (Berlin)* **526**, 135 (2014).
 - [34] H. M. Milchberg, S. J. McNaught, and E. Parra, *Phys. Rev. E* **64**, 056402 (2001).
 - [35] M. B. Smirnov and W. Becker, *Phys. Rev. A* **74**, 013201 (2006).
 - [36] F. Megi, M. Belkacem, M. A. Bouchene, E. Suraud, and G. Zwicknagel, *J. Phys. B: At. Mol. Opt. Phys.* **36**, 273 (2003).
 - [37] Th. Bornath, P. Hilse, and M. Schlanges, *Laser Phys.* **17**, 591 (2007).
 - [38] S. Micheau, H. Jouin, and B. Pons, *Phys. Rev. A* **77**, 053201 (2008).
 - [39] P. Hilse, M. Moll, Th. Bornath, and M. Schlanges, *Laser Phys.* **19**, 428 (2009).
 - [40] E. Ackad, N. Bigaouette, and L. Ramunno, *J. Phys. B: At. Mol. Opt. Phys.* **44**, 165102 (2011).
 - [41] I. I. Sobel'man, L. A. Vainshtein, and E. A. Yakubov, *Excitation of Atoms and Broadening of Spectral Lines*, 2nd ed. (Springer-Verlag, Berlin, 1995).
 - [42] M. V. Ammosov, N. B. Delone, and V. P. Krainov, *Zh. Eksp. Teor. Fiz.* **91**, 2008 (1986) [*Sov. Phys.-JETP* **64**, 1191 (1986)].
 - [43] F. A. Ilkov, J. E. Decker, and S. L. Chin, *J. Phys. B: At. Mol. Opt. Phys.* **25**, 4005 (1992).
 - [44] W. Lotz, *Z. Phys.* **206**, 205 (1967).
 - [45] L. M. Biberman, V. S. Vorob'ev, and I. T. Yakubov, *Kinetics of Nonequilibrium Low-Temperature Plasmas* (Consultants Bureau, New York, 1987).
 - [46] D. Kremp, M. Schlanges, and W.-D. Kraeft, *Quantum Statistics of Nonideal Plasmas* (Springer-Verlag, Berlin, 2005).

- [47] M. Schlanges, Th. Bornath, and D. Kremp, *Phys. Rev. A* **38**, 2174 (1988).
- [48] J. C. Stewart and K. D. Pyatt, Jr., *Astrophys. J.* **144**, 1203 (1966).
- [49] P.-G. Reinhard and E. Suraud, *Introduction to Cluster Dynamics* (Wiley-VCH Verlag, Weinheim, 2004).
- [50] J. D. Jackson, *Classical Elektrodynamics*, 3rd ed. (John Wiley & Sons, Hoboken, NJ, 1999).
- [51] Th. Bornath, M. Schlanges, P. Hilse, and D. Kremp, *J. Phys. A: Math. Gen.* **36**, 5941 (2003).
- [52] U. Kreibig and M. Vollmer, *Optical Properties of Metal Clusters* (Springer-Verlag, Berlin, 1995).
- [53] S. Link and M. A. El-Sayed, *Int. Rev. Phys. Chem.* **19**, 409 (2000).
- [54] M. Schlanges, Th. Bornath, V. Rietz, and D. Kremp, *Phys. Rev. E* **53**, 2751 (1996).
- [55] B. Schütte *et al.*, *Phys. Rev. Lett.* **112**, 253401 (2014).
- [56] S. P. Hau-Riege *et al.*, *New J. Phys.* **15**, 015011 (2013).
- [57] S. Byron, R. C. Stabler, and P. I. Bortz, *Phys. Rev. Lett.* **8**, 376 (1962).
- [58] D. Wanless, *J. Phys. B: At. Mol. Phys.* **4**, 522 (1971).
- [59] S. O. Kastner, *J. Quant. Spectrosc. Radiat. Transfer* **23**, 327 (1980).
- [60] <http://sprg.ssl.berkeley.edu/~mfgu/fac/>.
- [61] M. F. Gu, *Can. J. Phys.* **86**, 675 (2008).
- [62] M. Bitter *et al.*, *Phys. Rev. Lett.* **91**, 265001 (2003).
- [63] G. Y. Liang, G. Zhao, J. L. Zeng, and J. R. Shi, *Month. Not. R. Astron. Soc.* **350**, 298 (2004).
- [64] S. B. Hansen *et al.*, *Phys. Rev. E* **71**, 016408 (2005).
- [65] D. R. Lide (ed.), *CRC Handbook of Chemistry and Physics*, 80th ed. (CRC Press, New York, 1999).
- [66] O. Klein and S. Rosseland, *Z. Phys.* **4**, 46 (1921).
- [67] N. X. Truong *et al.*, *Phys. Rev. A* **81**, 013201 (2010).
- [68] P. Hilse, Th. Bornath, M. Moll, and M. Schlanges, *Contrib. Plasma Phys.* **49**, 692 (2009).
- [69] P. Hilse *et al.*, *Contrib. Plasma Phys.* **52**, 28 (2012).
- [70] J. Tiggesbäumker, personal communication, Universität Rostock.
- [71] F. Dorchie *et al.*, *Phys. Rev. E* **71**, 066410 (2005).
- [72] M. H. Chen, B. Crasemann, and H. Mark, *Atom. Data Nucl. Data Tables* **24**, 13 (1979).